Supporting information

Influence of junction resistance on spatiotemporal dynamics and reservoir computing performance arising from an SWNT/POM 3D network formed via scaffold template technique

Reservoir computing integration, internal state and discrimination

Reservoir integration is the process of incorporating external information or knowledge into the internal states of a reservoir computer. This can be done in several ways, depending on the specific task and application of the reservoir computer. One common approach is to use an external memory or buffer to store information that is relevant to the current input or task, and to incorporate this information into the internal states of the reservoir. This can be done by modifying the input weights or the reservoir weights, or by adding additional input or output connections to the reservoir. Another approach is to use external feedback connections to directly influence the internal states of the reservoir. This can be done by adding additional connections from the output of the reservoir back to the input or to the internal states of the reservoir. In general, reservoir integration can be used to improve the performance of a reservoir computer by providing additional information or context that can help to interpret the input or the internal states of the reservoir.

Reservoir states refer to the internal states of a reservoir computer, used for machine learning tasks such as time series prediction and chaotic systems modeling. The internal states of a reservoir computer can be represented as a high-dimensional dynamic system of equations, typically given by:

$$x(t) = f(W_{in}u(t) + W_{res}x(t-1) + b)$$

where x(t) is the internal state of the reservoir at time t, u(t) is the input to the reservoir at time t, W_{in} is the input weight matrix, W_{res} is the reservoir weight matrix, b is the bias vector, and f is the nonlinear activation function. The internal states of the reservoir are typically high-dimensional and complex and are difficult to interpret or understand.

The discrimination ability of a reservoir computer can be defined as the ability to separate or distinguish different inputs or input patterns based on their internal states. This is achieved using a readout layer, which maps the high-dimensional internal states of the reservoir to a lower-

dimensional output space. The readout layer can be trained to respond differently to different inputs, allowing the reservoir computer to perform tasks such as classification or pattern recognition. The readout layer can be represented as a linear transformation:

$$y(t) = W_{out}x(t) + c$$

where y(t) is the output of the reservoir at time t, W_{out} is the output weight matrix, and c is the output bias vector.
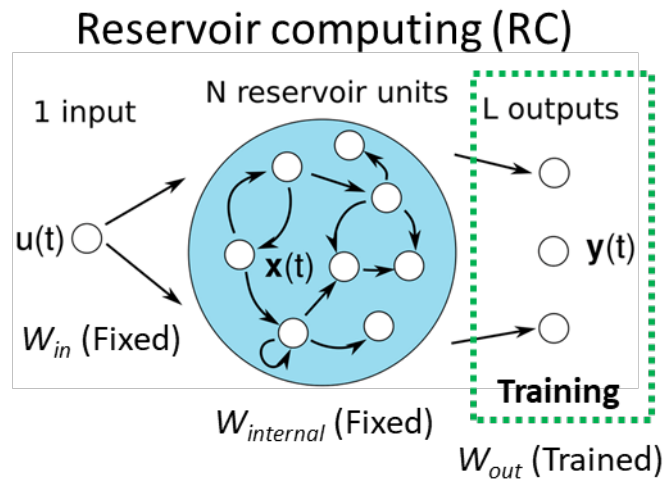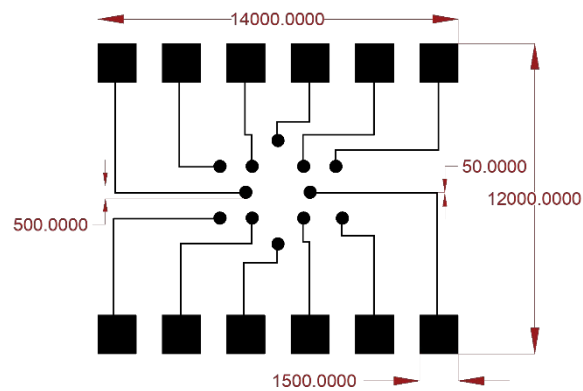

Figure S1. Schematic of reservoir computing.

Figure S2. Microelectrode array (MEA) schematic used for 2D device fabrication. The electrode array was fabricated using photolithography and chemical etching. The unit for all values shown are Micrometer (μm).
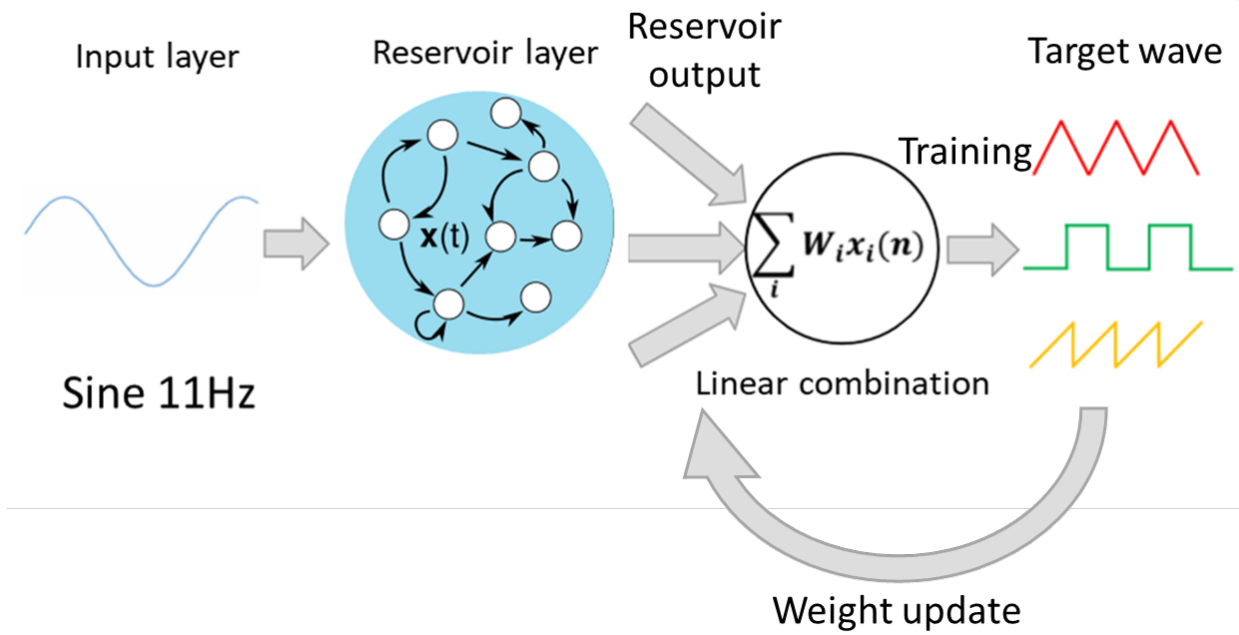
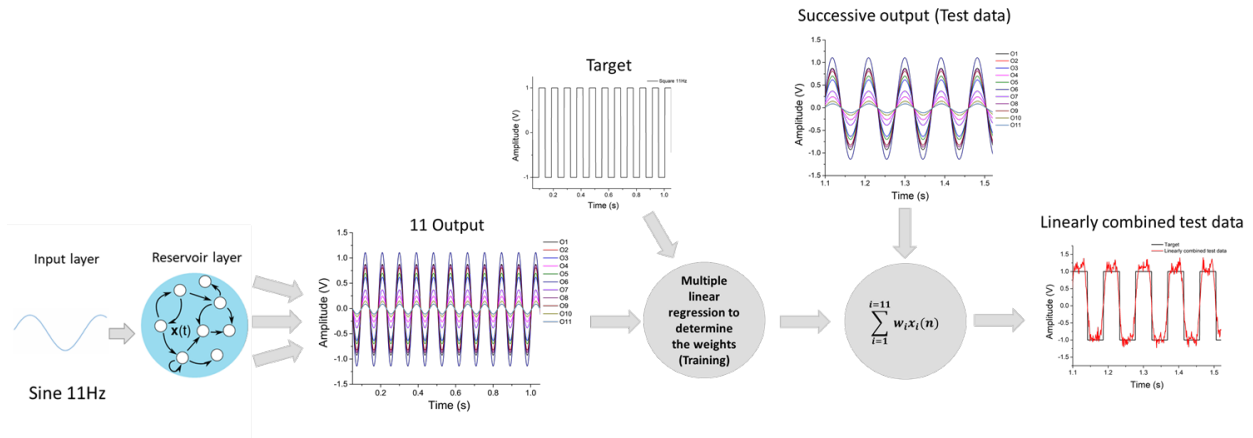*Figure S3 The methodology for waveform generation benchmark task.*

Figure S4. 3D device waveform generation task with 3 VPP 11-Hz sinusoidal input and square wave target (one out of five samples).
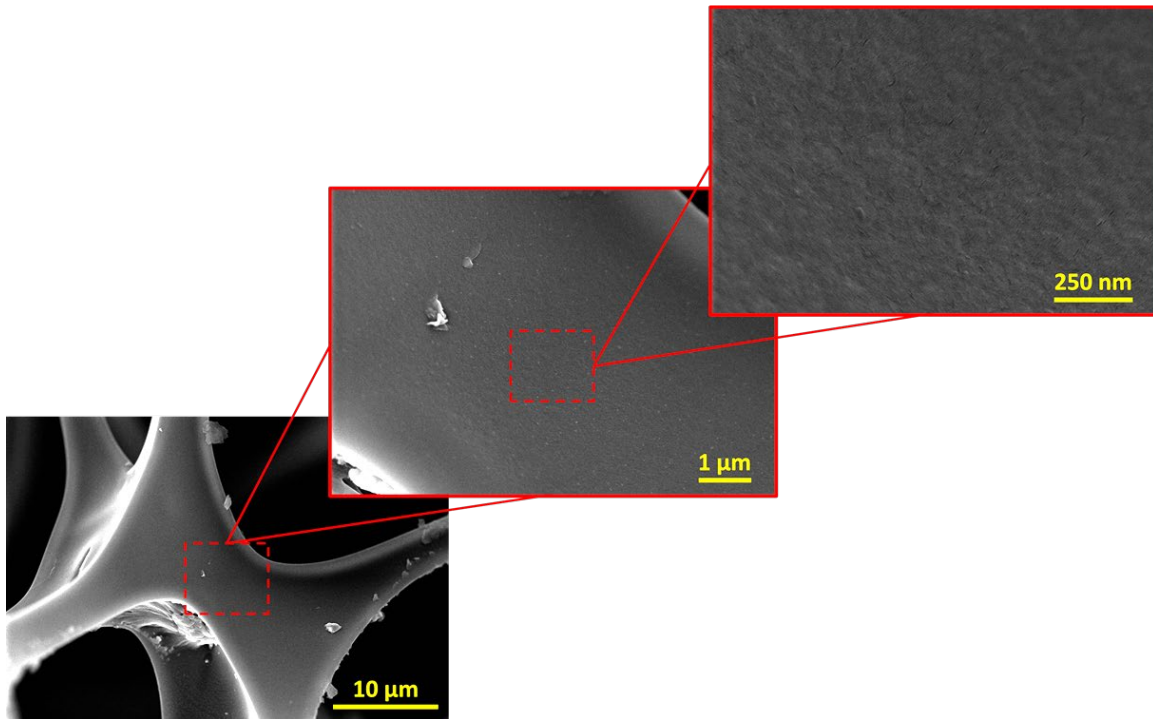

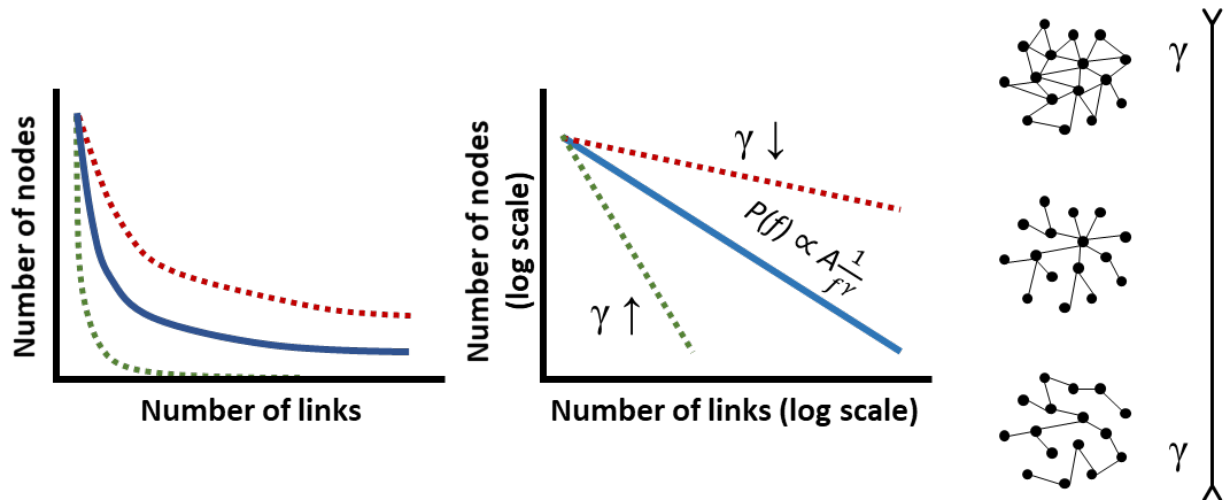*Figure S5. FESEM image of pristine (blank) melamine foam.*

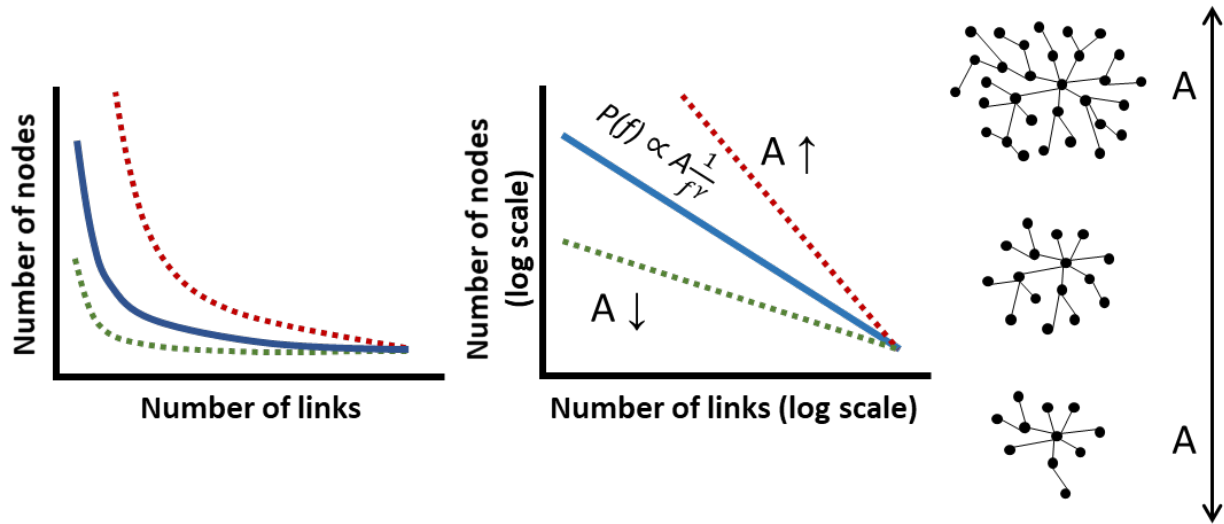*Figure S6. Correlation of γ with scale free network topology.*

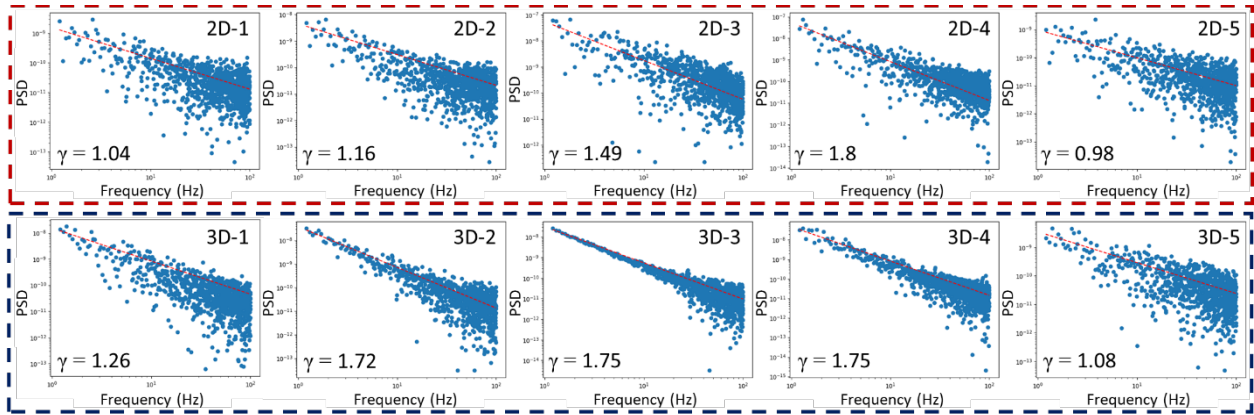*Figure S7. Correlation of A with scale free network topology.*

Figure S8. The 1/f fitting of PSD data obtained from five samples of 2D (red box) and five samples of 3D (blue box) devices with 3V DC input, calculated using Eq. 1.
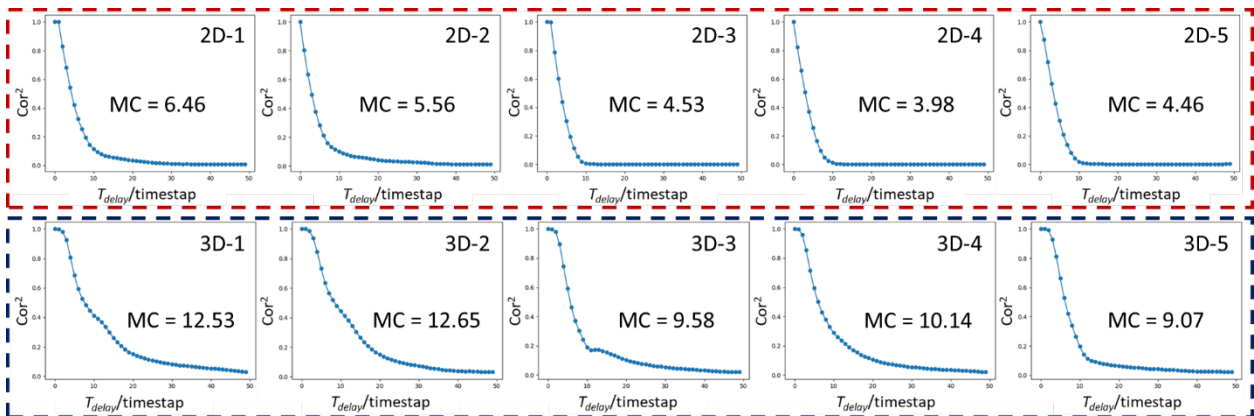

Figure S9. The memory capacity plot obtained from five samples of 2D (red box) and five samples of 3D (blue box) devices with random pulses of zeros and ones as input, calculated using Eq. 2.
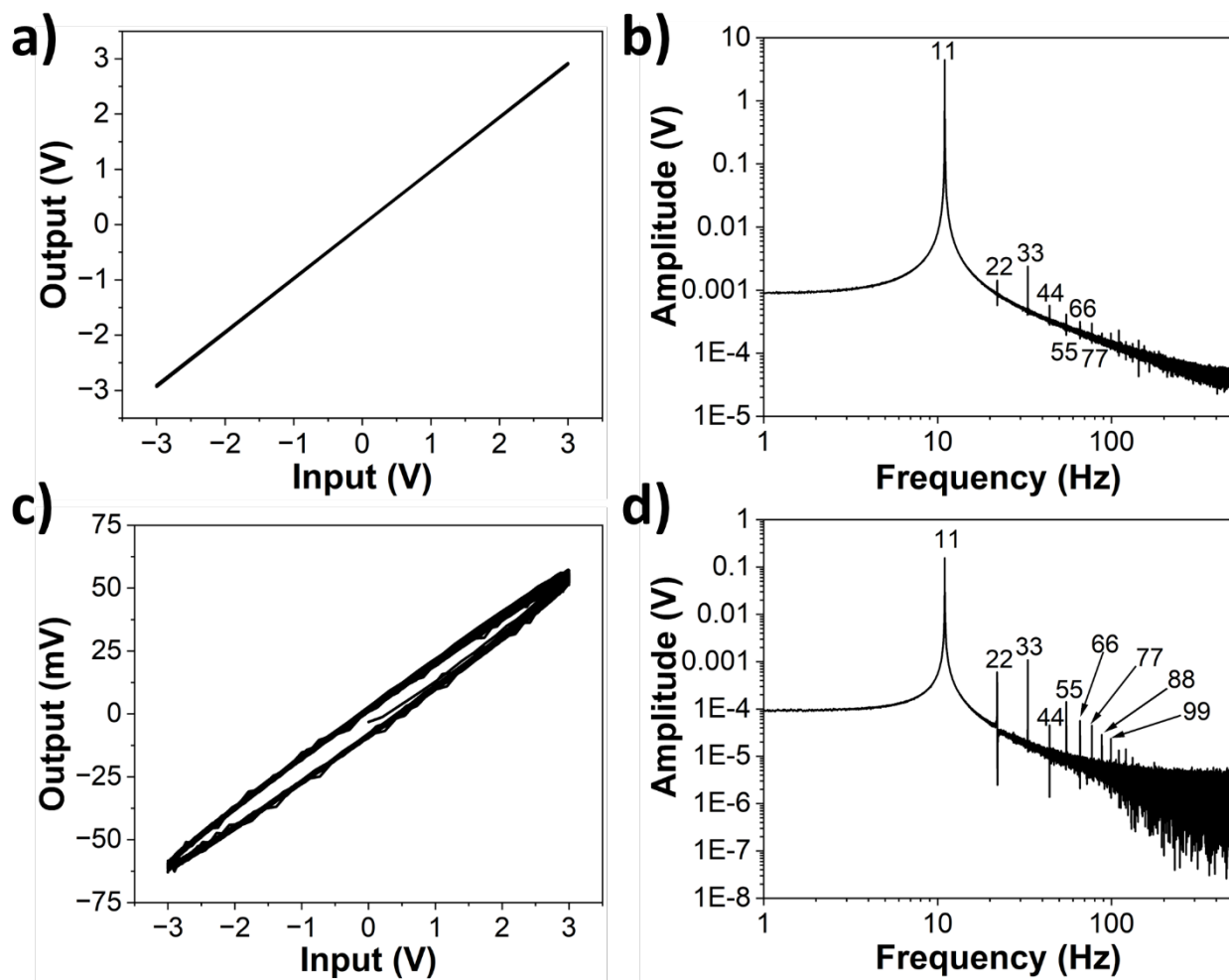
Figure S10. Lissajous plot of a) 2D and c) 3D devices obtained by plotting the input and output data collected from 3 V 11-Hz AC signal input; FFT plot of b) 2D and d) 3D devices obtained from 3 V 11-Hz AC signal input.
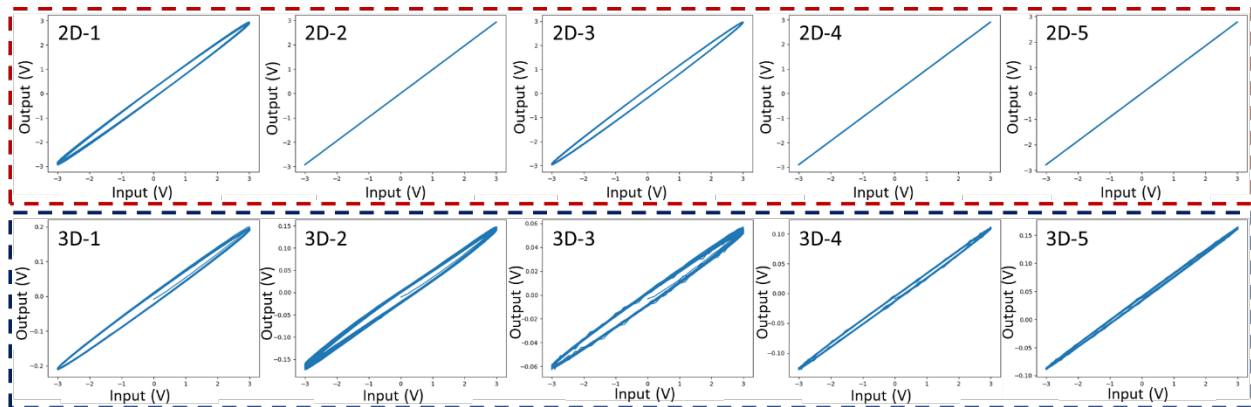
Figure S11. The Lissajous plot obtained from five samples of 2D (red box) and five samples of 3D (blue box) devices with 3 V 11-Hz AC input.
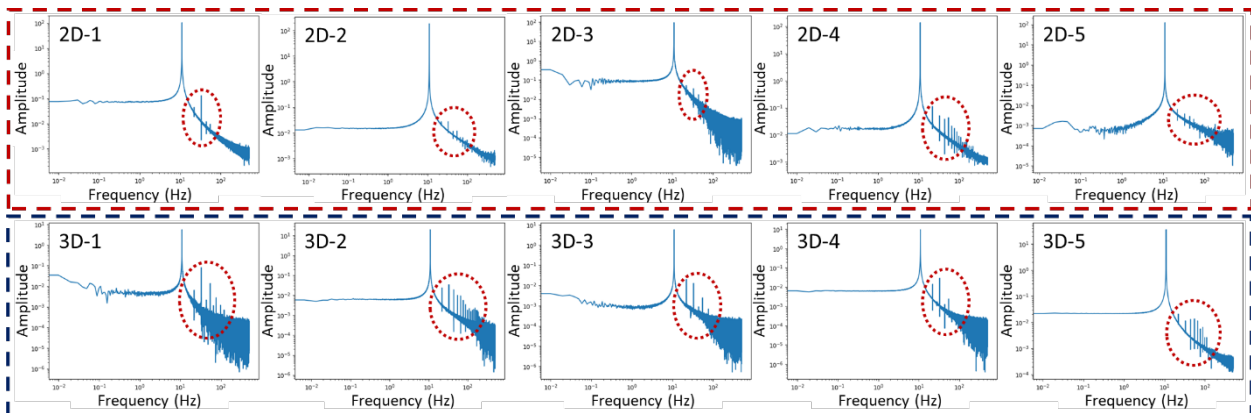

Figure S12. The FFT plot obtained from five samples of 2D (red box) and five samples of 3D (blue box) devices with 3 V 11-Hz AC input. Red dashed circle exhibits the higher harmonics.

a)

Z (KΩ)

Resistance (Ω)

Capacitance (F)

b)

Φ (°)

Resistance (Ω)

Capacitance (F)

C

c)

1 mF
1 Ω

V_{out} (V)

V_{in} (V)

Z = 0.99762 Ω
Φ = -3.9537 °

d)

1 mF
1 MΩ

V_{out} (V)

V_{in} (V)

Z = 14.4686 Ω
Φ = -89.999 °

e)

1 nF
1 Ω

V_{out} (V)

V_{in} (V)

Z = 1 Ω
Φ = -3.96 °

f)

1 nF
1 MΩ

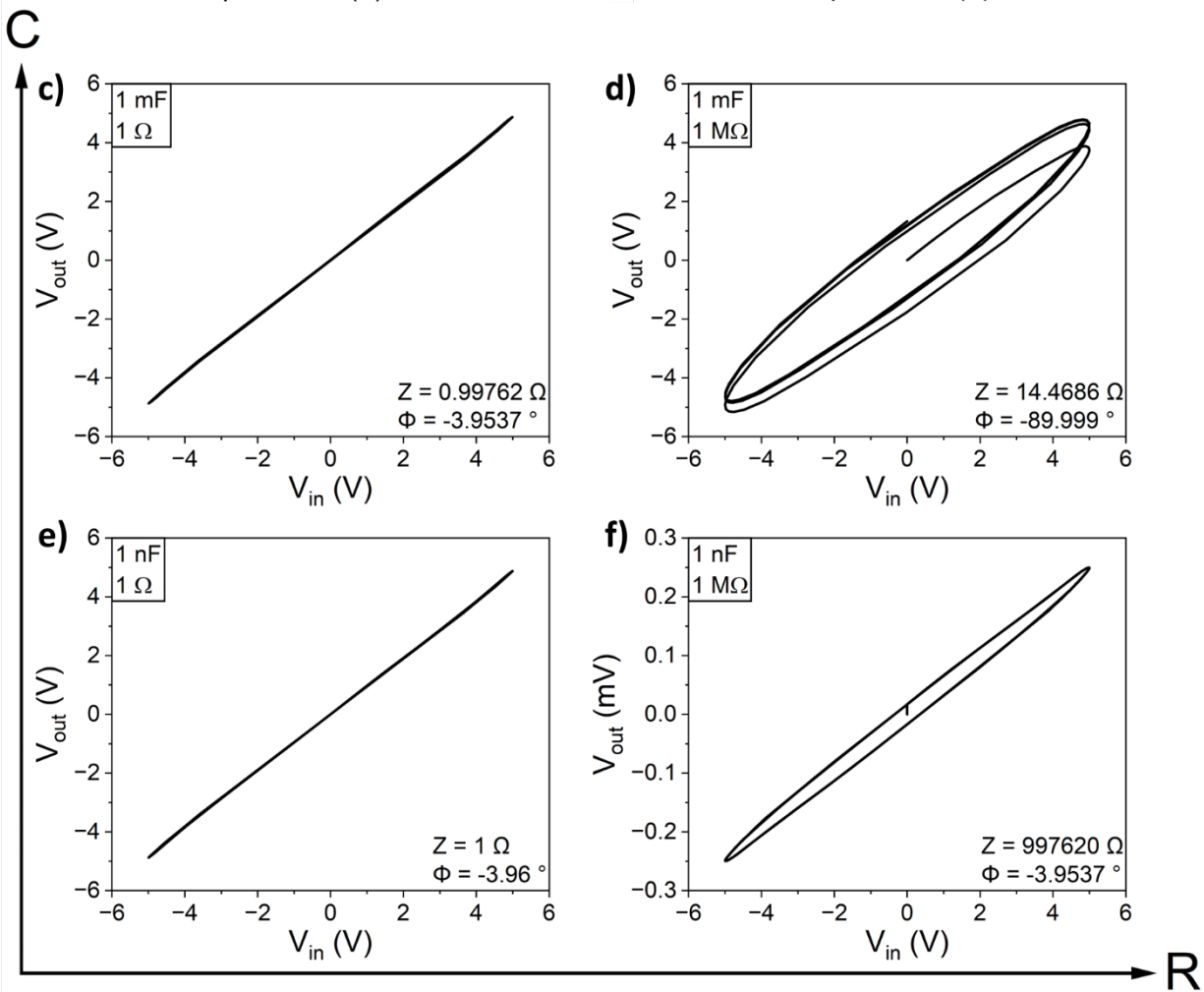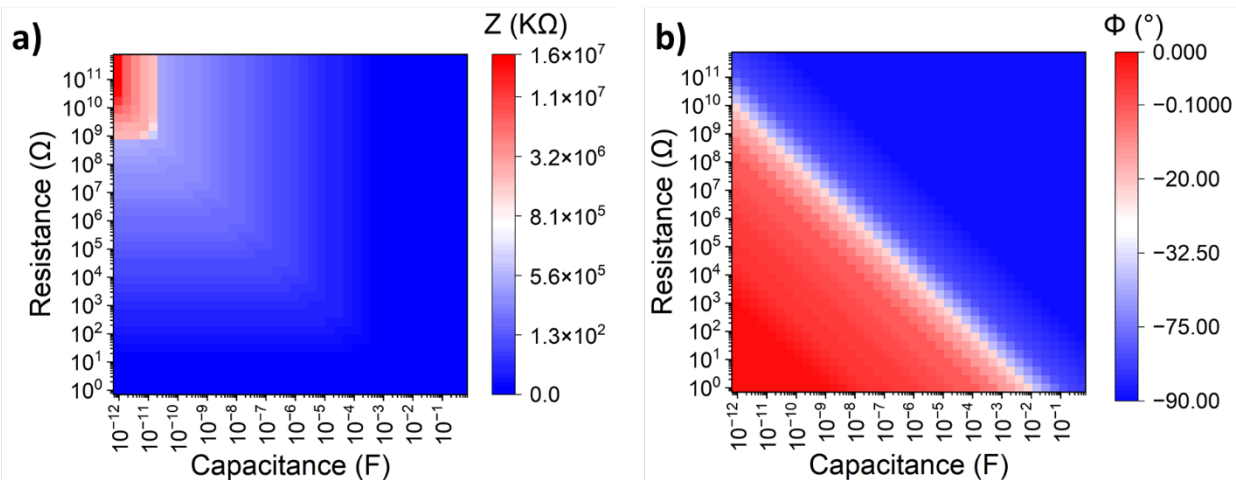V_{out} (mV)

V_{in} (V)

Z = 997620 Ω
Φ = -3.9537 °

R

Figure S 13. Correlation of resistance (R) (SWNT junction resistance) and capacitance (C) (interface between SWNT and POM) in parallel RC circuit [1–3] with a) Impedance (Z) and b) phase angle (Φ). The increase in capacitance (C) or resistance (R) increase the phase angle (Φ) while the impedance (Z) is mainly affected by change in resistance. It is evident from LTspice XVII simulation results shown in figures c), d) and e), f) that the increase in junction resistance (R) increase the nonlinear spatiotemporal dynamics of the device. On the other hand, we can see that the less amount of interface between SWNT and POM represented by smaller C value (1nF) results in lower output voltage in the device with higher junction resistance (figure f) which is not evident in the device with lower junction resistance (figure e) which exhibits nearly no spatiotemporal dynamics. This behavior can be explained by considering the impedance (Z) and phase angle (Φ). In c) and d) as junction resistance increases the Z slightly and Φ drastically increase resulting in a prominent spatiotemporal dynamic while in e) and f) although the Φ is nearly the same the Z increase drastically resulting in smaller current flow between input and output electrodes. Considering that C is the same in e) and f) and $I_C = C\frac{dV}{dt}$ we could conclude that $I_C = \frac{dV}{dt}$ and the current drop results in slower rate of voltage change resulting in the presence of relatively more distinct spatiotemporal dynamics.

Waveform generation

Fourier series use infinite series of periodic sinusoid functions of different coefficients to produce complex periodic functions with other forms such as sawtooth (Equation S1) and square wave (Equation S2). It is evident that to construct a sawtooth wave, long-range of both odd and even harmonics are required, while from the FFT data (Figures S8b, S8d, and S10), it is clear that some samples exhibit very short-range harmonics with stronger odd harmonics intensity than the even. As a result, the waveform generation task, particularly with the sawtooth wave target, shows the observed result. On the other hand, the square wave requires a long-range of odd harmonics, and since odd harmonic intensities are stronger in the samples, reconstruction of the target wave results in higher accuracy.

$$Sawtooth = f(x) = \frac{1}{2} - \frac{1}{\pi}\sum_{i=1}^{\infty}\frac{1}{n}sin\left(\frac{n\pi x}{L}\right) \qquad\qquad (Eq.\,S1)$$

$$Square = f(x) = \frac{4}{\pi}\sum_{i=1,3,5\dots}^{\infty}\frac{1}{n}sin\left(\frac{n\pi x}{L}\right) \qquad\qquad (Eq.\,S2)$$
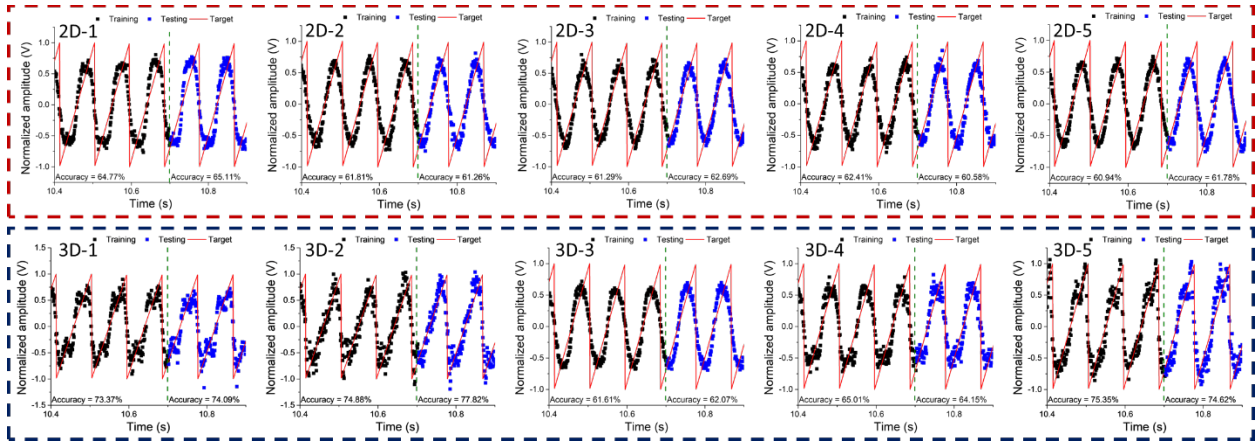
Figure S14. The waveform generation for 11-Hz sawtooth target wave obtained from five samples of 2D (red box) and five samples of 3D (blue box) devices with 3 V 11-Hz sinusoidal input.
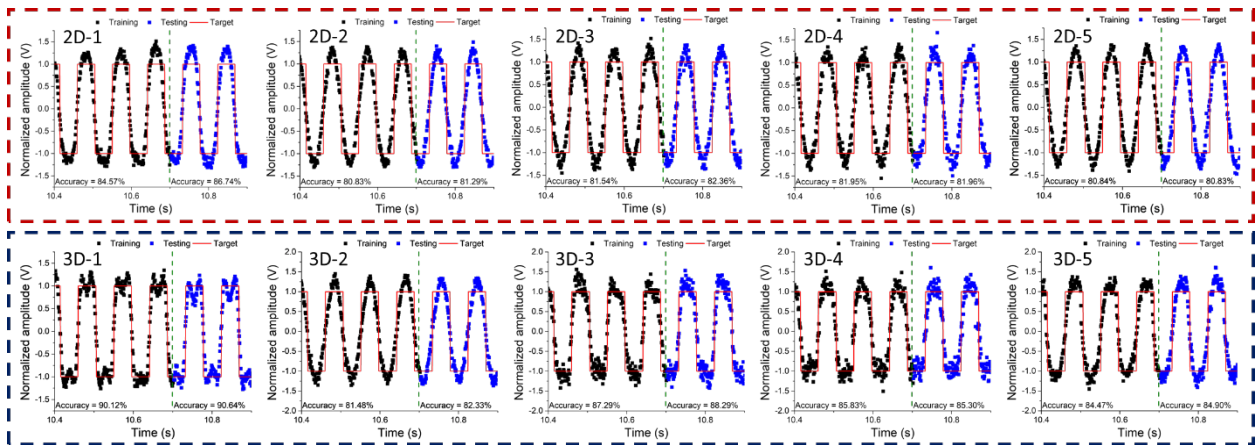

Figure S15. The waveform generation for 11-Hz square target wave obtained from five samples of 2D (red box) and five samples of 3D (blue box) devices with 3 V 11-Hz sinusoidal input.
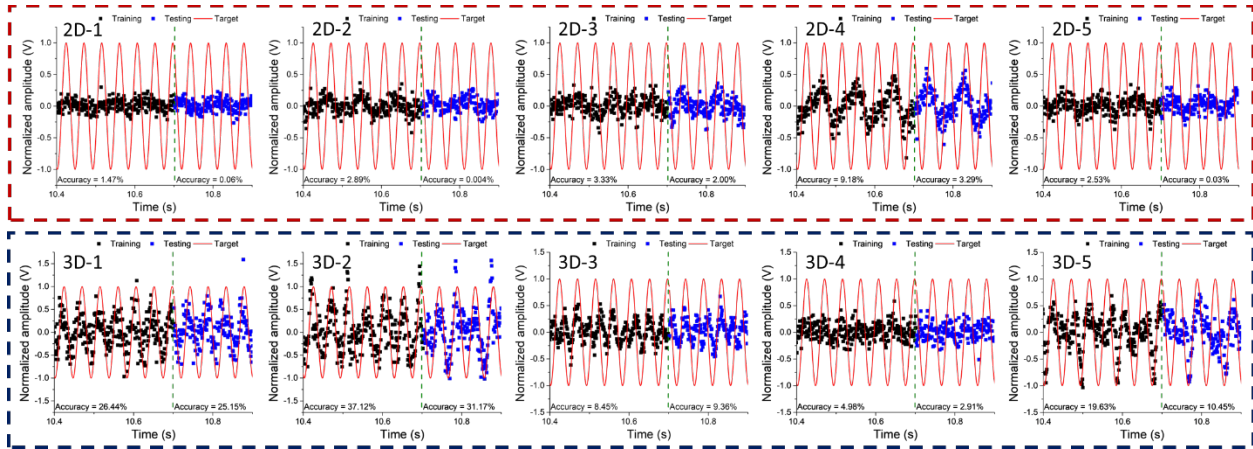
Figure S16. The waveform generation for sine 22-Hz target wave obtained from five samples of 2D (red box) and five samples of 3D (blue box) devices with 3 V 11-Hz sinusoidal input.
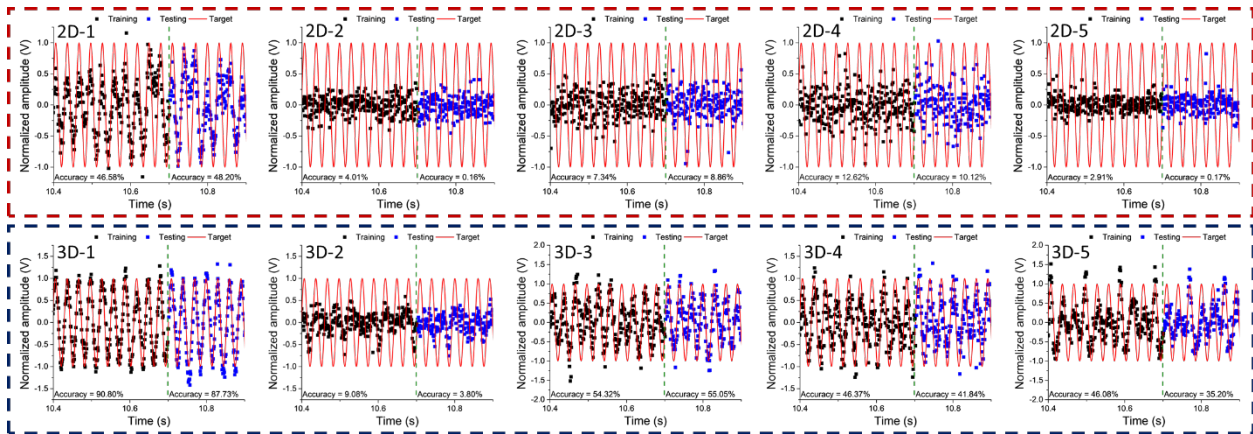

Figure S17. The waveform generation for sine 33-Hz target wave obtained from five samples of 2D (red box) and five samples of 3D (blue box) devices with 3 V 11-Hz sinusoidal input.

References

1) Hu, J., Ji, Y., Chen, W., Streb, C. & Song, Y.-F. Energy Environ. Sci. **9**, 1095 (2016).

2) Banerjee, D., Kotooka, T., Azhari, S., Usami, Y., Ogawa, T., Gimzewski, J. K., Tamukoh, H. & Tanaka, H. Adv. Intell. Syst. **4**, 2100145 (2022).

3) Holm, S., Holm, T. & Martinsen, Ø. G. PLoS One **16**, e0248786 (2021).